J Polym Res (2012) 19:9839
DOI 10.1007/s10965-012-9839-z

ORIGINAL PAPER

Physical characterizations of semi-conducting conjugated polymer-CNTs nanocomposites

M. Abu-Abdeen · Ayman S. Ayesh · Abdullah A. Al Jaafari

Received: 19 September 2011 / Accepted: 9 February 2012

Abstract Carbon nanotubes (CNTs) were prepared using Alcholic Catalyst Chemical Vapor Deposition (ACCVD) technique in order to investigate the effects of their addition on the optical, electrical and mechanical properties of Poly (3-octylthiophene-2,5-diyl) (P3OT) matrix. The absorption spectra of the prepared CNTs and CNT-P3OT nanocomposites were measured in the spectral range 200 nm–3,000 nm at room temperature. The optical energy gap was determined from the obtained UV/Vis absorption spectrum. Optical results reveal that the prepared CNTs are almost single walled. Besides, the addition of CNTs to P3OT polymer matrix will decrease the optical energy gap and enhance the optical absorbance of P3OT matrix. On the other hand, the addition of CNTs to P3OT matrix will increase the electrical conductivity of P3OT matrix up to four orders of magnitude above the percolation threshold (0.44 wt% CNTs). Additionally, I–V characteristics indicate that the conduction mechanism is Ohmic at low applied voltage range while it is due to the trap charge limited at high applied voltage range. Furthermore, the behavior of dc conductivity with temperature was also investigated and the obtained results reveal that the activation energy decreases with CNTs content. Finally, mechanical results reveal that the elastic modulus values increase with the increasing of CNTs content in P3OT matrix.

M. Abu-Abdeen · A. S. Ayesh (✉) · A. A. Al Jaafari
Department of Physics, College of Science,
King Faisal University,
P.O.B 400, 31982 Al-Ahsa, KSA
e-mail: dr_ayesh67@yahoo.co.uk

M. Abu-Abdeen
Department of Physics, College of Science, Cairo University,
Giza, Egypt

Published online: 01 March 2012

Keywords ACCVD · CNTs · P3OT · Optical · Dc conductivity · Stress–strain

Introduction

The synthesis of nanocomposites opens up an attractive route to obtain novel and optimized compounds that can meet a broad range of applications. In this situation, the exceptional properties of nanoparticles have made them a focus of widespread research in nanocomposite technology [1–3].

Conjugated polymers such as P3OT have been extensively studied [1–14] as promising materials for applications in light-emitting diodes, displays, solar cells or other optoelectronic devices due to their processability, flexibility and low production costs. On the other hand, many important aspects of the electronic and optical properties of these materials are still not fully resolved [6–11]. However, conjugated polymers can become electrically conducting by doping or oxidation process but are usually insoluble in common solvents. One method to convert them into soluble is to add lateral groups to the backbone of the molecules, such as the case of poly3-octylthiophene (P3OT). The advantage of a soluble conducting polymer is evident for application purpose. Like many polyalkylthiophenes (PATs), P3OT can be obtained as thin films by electrochemical polymerization of 3-octylthiophene (3OT) [13].

Single walled carbon nanotubes (SWCNTs) can be described as a single graphene sheet rolled into tube. These tubes are proposed to be either metallic or semiconducting depending on their spiral conformation and diameter, making them ideal reinforcing fillers composite materials [14]. Additionally, the unique electronic and mechanical properties of carbon nanotubes (CNTs) have shown a lot of potential for a vast

range of applications, including quantum wire for scanning probe microscopy and molecular diodes [12–21].

Recently, research has focused on composites of electronically active conjugated polymers and carbon nanotubes, which demonstrate a number of advantages. They show potential for electronic device applications promising to greatly enhance transport properties in these systems. This is thought to be a key issue for the realization of viable devices such as organic light emitting diodes and solar cells [12–17]. Despite of the extensive researches on these composites, still more researches need due to the following reasons: (a) practical advantages of CNT-polymer composites is the case in the preparation of products with shapes and patterns by using simple processing technology and hence reduces the manufacturing costs and (b) their electronic and optical properties are still not fully resolved [13–17].

Different attempts have been also made to disperse uniformly CNTs for the preparation of the polymer composites such as using functionalized CNTs, in situ polymerization and sonification in organic solvents. Besides, chemical functionalization of carbon nanotubes using different strong acids, generally, will introduce carboxylic groups at CNTs surface and consequently, this will improve CNTs dispersion in organic solvents or polymer matrix. At the same time, such a method will cause a morphological damages to CNTs and will cause physical damages in addition to the severe degradation of the originally desirable properties of CNTs. Consequently, casting technique with the using of ultrasonication method to disperse CNTs in polymer matrix is non-distructive method and will not introduce any chemical modifications in the polymer-CNTs composites [18, 19].

Present work aims to prepare CNTs-semiconducting conjugated polymer nanocomposites with significant physical properties for photovoltaic applications. In this respect, the absorption spectra of these nanocomposites will be investigated. Besides, the percolation concentration threshold of CNTs will be calculated from the dc conductivity measurements. The conduction mechanisms and the temperature dependence of the dc conductivity will also be studied. In addition, stress–strain curves will be studied and some of the mechanical parameters will be calculated. Finally, correlations between these studied physical properties will be discussed.

Experimental

Materials and preparation

Polymer

Poly(3-octylthiophene-2,5-diyl) (P3OT) was purchased from Aldrich (Ref. No. 445711). It has greater than 98.5% head-to-tail region-specific conformation, molecular weight 34,000, melting point 90 °C, and fluorescence emission at 562 nm in chloroform when the excitation wavelength is 442 nm.

Synthesis of CNTs

Carbon nanotubes (CNTs) were synthesized via the alcohol catalytic chemical vapor deposition (ACCVD) technique using a 50 cm long ceramic tube furnace with diameter of 12 cm. Cobalt acetate supported catalyst was first prepared. A metal acetate solution was prepared by dissolving 42 mg of cobalt acetate $(CH_3COOH)_2Co\text{-}4H_2O$ (99.999%, Sigma-Aldrich) in 10 ml of ethanol with stirring for 10 min followed by sonication for 2 h at room temperature. For a substrate, we employed p-type Si wafer with (100) surface polished at one surface (University Wafers, USA) and a thickness of 0.5 mm. The substrate was cut into a strip of about 10×25 mm^2. The substrate was cleaned by consecutive acetone sonication for 5 min, washed with DI water and blown with dry nitrogen. The substrate piece was then submerged vertically into the prepared metallic acetate solution for 5 min. This piece was then drawn up from the solution at a constant speed of 4 cm/min. The piece was then placed in a furnace and maintained at 400 °C for 5 min [20].

For the growth of CNTs, Cobalt acetate supported catalyst was placed into alumina combustion boat; whereas a 10° inclined graphite stage was used to support the substrates and the group was then placed at the center of the tube furnace. The tube was evacuated to 150 mTorr, and samples were heated to the desired reaction temperature under 250 sccm of flowing argon. Once the growth temperature was reached (depending on the growth temperature), samples were held at that temperature for 5 min. The argon was then shut off and the tube was evacuated before the introduction of alcohol vapor. The alcohol vapor (ethanol) was then transferred into the tube furnace to achieve a pressure of 5–10 Torr. After growth, the alcohol vapor was evacuated, argon was introduced again and the reaction tube was cooled to room temperature. CNTs growth time was kept constant at 50 min unless otherwise stated [21]. A TEM Image of the synthesized CNTs is shown in Fig. 1.

Preparation of polymer nanocomposites

P3OT was dissolved in chloroform with ultrasonication up to 30 min. At the same time, the required amount of CNTs was dispersed in chloroform and sonicated for 30 min to obtain dispersed nanotubes suspension without any chemical pre-treatment to avoid any morphological damages to these nanotubes. Both solutions were mixed together and further sonicated for 2 h to give a stable solution with no detectable solid precipitations. The resulting solution was poured to a completely horizontal betray dish and then dried

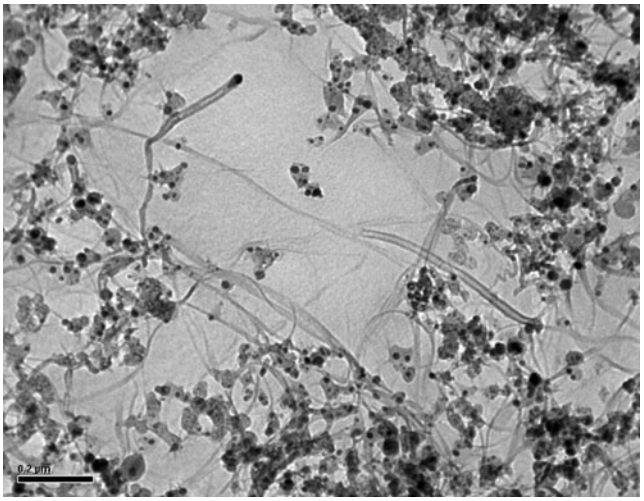

Fig. 1 TEM micrograph of the prepared CNTs

at room temperature. The dried film was then heated up to 50 °C in order to remove remnant solvent. Such a preparation method, however, leads to a uniform dispersion of CNTs in P3OT matrix without any morphological dameges and both components (P3OT and CNTs) are physically bonded to each other [17, 18]. A series of composite films were prepared at different weight ratios (0–5 wt%) of CNTs/P3OT.

Transmission electron microscope (TEM)

The prepared CNTs powder was sonicated in methanol and placed onto holey/lacey carbon coated copper grids for TEM (Model 1011 JEM at 100 KV KSU, Saudi Arabia) observations to confirm both their existence and morphology, as shown in Fig. 1.

Optical properties

The absorption spectra of CNTs and CNT-P3OT composites in the UV-Visible and NIR regions were measured using a Shimadzu UV- VIS spectrophotometer Model UV-3600, Japan in the wavelength range 200–3,000 nm. The scan step was 0.5 nm. The optical absorbance (A) spectra of samples were collected at room temperature. The absorption coefficient α was calculated from the absorbance (A). After correction for reflection, α was calculated using the relation [22]:

$$I = I_0 \exp(-\alpha x) \tag{1}$$

$$\alpha(\upsilon) = \frac{2.303}{x} \log\left(\frac{I}{I_0}\right) = \frac{2.303}{x} A(\upsilon) \tag{2}$$

where I_0 and I are the incident and transmitted intensity, respectively, and x is the sample thickness.

DC conductivity measurements

The samples employed for I–V and conductivity measurements were shaped into circular discs of diameter 10 mm and thickness of 0.1 mm. Each sample was coated with Aluminum and placed inside an electric oven which operates up to 160 °C with an automatically controlled temperature.

The dc current measuring equipment comprised a digital electrometer (model 6517A, Keithley), 50 V DC power supply (512–65 LEYBOLD), coaxial cable, metal shielding, and a common ground loop (to eliminate electrical noise).

Mechanical properties

The stress–strain tests were carried out on a DMA Q800 machine TA instruments (USA), using the tension film clamping arrangement. Specimens in the form of films with dimensions 15 mm length, 4 mm width and 0.1 mm thick were used.

Results and discussion

UV-visible-NIR absorption spectra

Prepared carbon nantubes

One of the power full analyses used to recognize both the existence and quality of SWCNTs is UV-visible and NIR spectra [22–24]. Jeong, M.S. and Byeon, C.C [23] reported that the absorption spectrum of SWCNT mainly consists of three absorption peaks. The first peak at around 0.8 eV and the second is around 1.5 eV. These two peaks correspond to absorption characteristic of semiconducting SWCNT. The third peak at around 2 eV corresponds to metallic SWCNT. Besides, Kim, D.Y. et al. [24], showed that the optical absorbance increases with increasing average CNT length. However, in the present work, the absorption spectra of prepared CNTs (at 800 °C) were measured in the spectrum range 200–3,000 nm as shown in Fig. 2. Figure 3 shows the absorbance spectra as a function of photon energy at NIR region. It is clear from Fig. 3 that there are two peaks (peak I and peak II) at around 0.78 eV and 1.35 eV which represent the characteristic peaks of SWCNT [23]. From the obtained results, we can say that the grown CNTs are almost single walled type.

Furthermore, Chen, D. et al. [25], reported that semiconducting SWCNTs has a direct band-gap and the value of the optical energy gap is located in the range from 0.5 eV up to above than 1 eV. However, in the present work we use Mott, Davis, and Tauc formula [22, 26] to determine the optical energy gap. It was found that the transition type is direct with r=0.5 (Fig. 4) and the value of the optical energy gap is

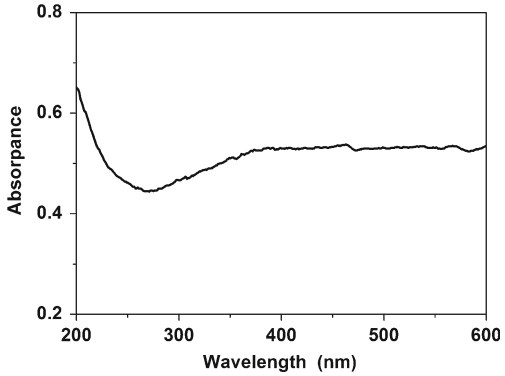

Fig. 2 UV-visible absorbance spectrum of prepared CNTs

about 1.16 eV. This result is in a good agreement with those reported by Chen, D. et al. [25]. This indicates that the prepared CNTs are almost semiconducting SWCNTs.

CNT-P3OT composites

Koizhaiganova, R.B et al. [1] reported that P3OT polymer solution and films themselves can show different absorption spectra when prepared using different solvents. However, Fig. 5 shows the absorption spectra of CNT-P3OT nanocomposite films for various concentrations of CNTs. The absorption spectra do not show any significant change from that of the P3OT polymer up on adding nanotubes up to 1 wt %. The CNTs characterstic peaks can be clearly observed when the concentration of CNTs is equal or above 1 wt% [23]. It is also clear that the appearnce of CNTs characterstic peaks depends on the optical volume of the P3OT matrix. Usually, new absorption peaks are expected if there is a ground-state electronic interaction between the two components in a composite matrix. In CNT-P3OT nanocomposites, the absence of new absorption peaks indicates the absence of significant electronic interaction in the ground state between CNTs and P3OT matrix [1, 13]. Additionally, in the domain wavelength region, addition of CNTs to P3OT matrix will enahnce the absorpance of P3OT matrix specially at visible and NIR regions.

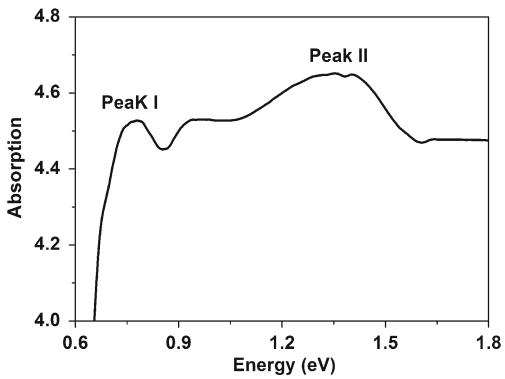

Fig. 3 NIR spectrum of prepared CNTs

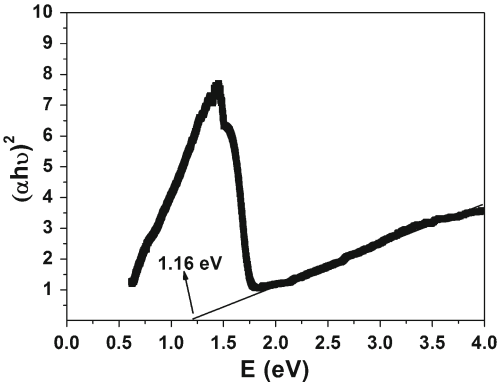

Fig. 4 $(\alpha h\acute{\upsilon})^2$ versus photon energy (eV) for the prepared CNTs

The optical energy gap for CNTs-P3OT nanocomposites was also detrmined using Mott, Davis, and Tauc formula [22, 26], see Figs. 6 and 7. All composites show direct band gap with r=0.5. Furthermore, addition of CNTs to P3OT matrix will decrease the optical energy gap from 2.74 eV (for P3OT) up to 2.51 eV (for 5% CNT). This decrease is also reported elsewhere by other resrcheares [1, 13]. Such a decrease could be attributed to the fact that increasing CNTs in the P3OT matrix will increase the formation of localized states in the forbidden gap [22, 26].

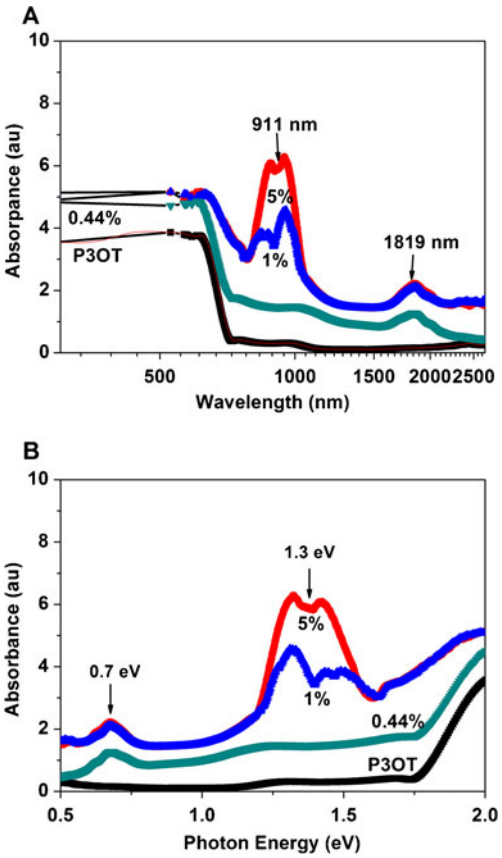

Fig. 5 Absorbance spectra of CNT-P3OT composites: a versus wavelength and b versus photon energy

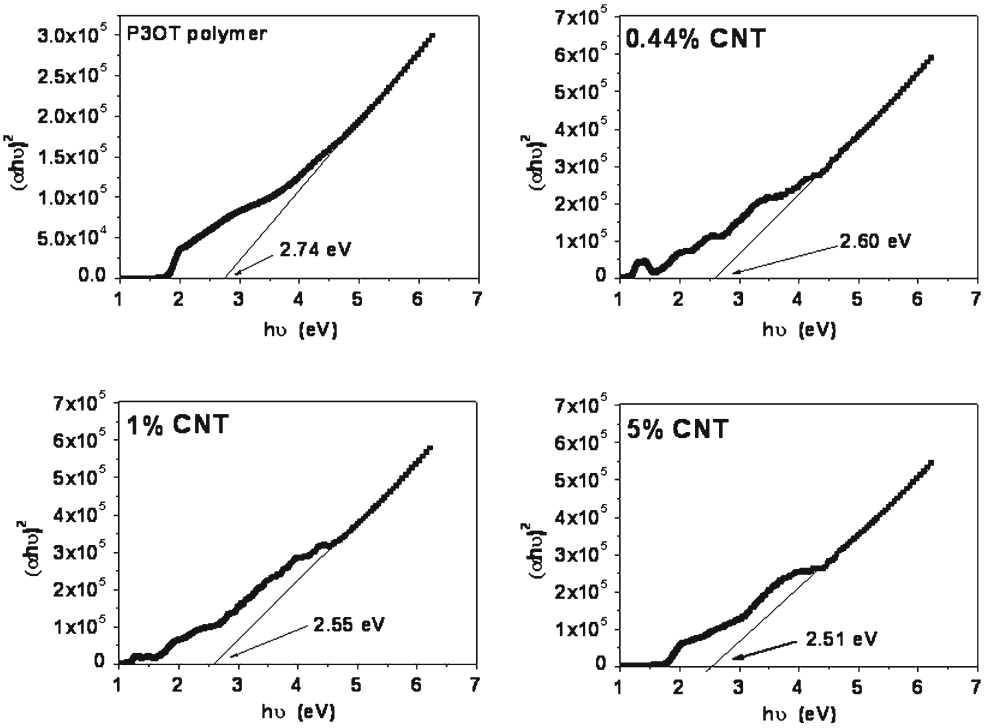

Fig. 6 $(\alpha h\upsilon)^2$ versus photon energy (eV) for CNT-P3OT composite films

Electrical characterization

The room temperature conductivity of the CNT-P3OT nanocomposites is shown in Fig. 8 as a function of the weight fraction of CNTs in P3OT.

Generally, conductivity depends on the polymer matrix and the filler materials. With regard to the polymer, it is controlled mostly by the conjugation and the dopants present in them [1, 13]. If the filler material is CNTs, it is decided by its purity, alignment, and the concentration. In such composites, the polymer layer in the internanotube connections presents highly resistive section in the electrical pathway, acting as a barrier to efficient carrier transport between the nanotubes and models fluctuation-induced tunneling for the conductivity [1]. In other words, when the distance between nanotubes becomes sufficiently small for electrons to tunnel through the polymer or for many physical contacts between nanotubes to be formed, the electrical response of the composites is then described by percolation theory, Eq. 3, and the CNTs concentration that marks this insulator-conductor transition is referred to as the percolation threshold (Pc) [13]:

$$\sigma = C[P - P_c]^t \tag{3}$$

where σ is the composite conductivity, P the weight fraction of nanotubes in the composites, C is a constant, and t is a critical exponent.

As shown in Fig. 9, the introduction of nanotubes does increase the conductivity of the composites by up to four orders of magnitude. This result suggests that the formation of network structure between nanotubes in the polymer

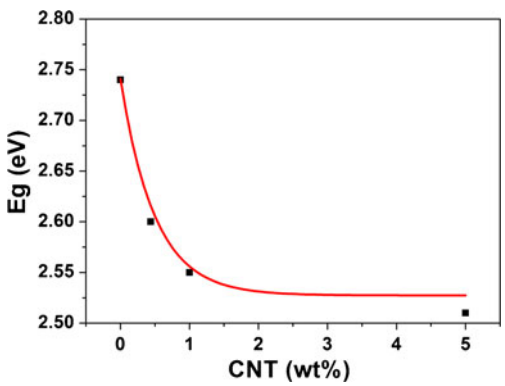

Fig. 7 Optical energy gap versus CNT concentration for CNT-P3OT composite films. *Solid line* represents the exponential fitting

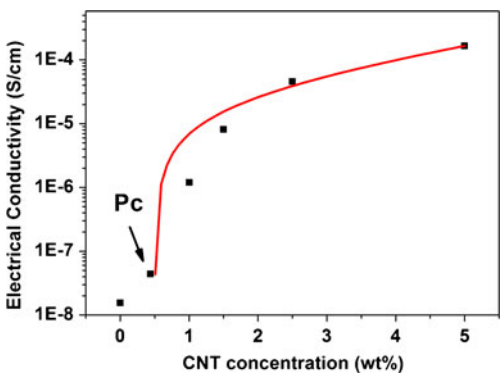

Fig. 8 Electrical conductivity variations versus weight fraction of CNTs in the composites. The *solid line* is a fit to the power law (Eq. 3)

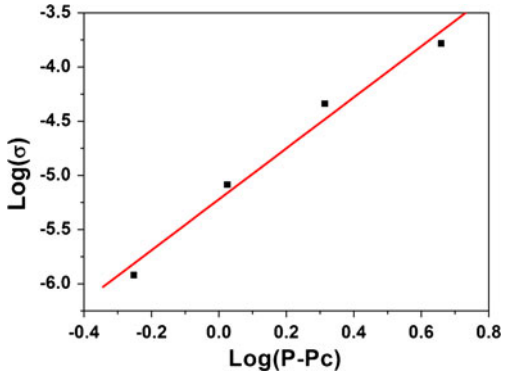

Fig. 9 Plot of log (σ) versus log (P-Pc) for CNT- P3OT composites at room temperature

matrix and this facilitates the electron transport through tunneling throughout the polymer or by electron, hopping along CNTs interconnects [1]. Besides, Fig. 9 shows the linear relation between log(σ) and log (P-Pc) in accordance to Eq. 3, where the percolation threshold for CNTs-P3OT nanocomposites (Pc) turns out to be 0.44 and the value of the exponent (t) is 2.35. However, the final result indicates that CNTs are percolated above 0.44% CNTs in P3OT matrix.

The charge transport mechanism based on the power law model $I \approx V^m$ has been widely used for the analysis of the conduction phenomenon in organic or polymeric materials [27–34]. The model is divided into three regimes, Ohmic ($m=1$), trap-free space charge limited ($m=2$), trap charge limited ($m>2$) [32]. However, Fig. 10 presents a nonlinear log(I)-log(V) characteristic curves of the studied composite samples. It is interesting to note that in all cases the points fall on two intersecting straight lines of unequal slopes which indicates the existence of two different conduction mechanisms. The first one operates at low applied voltages (slope 1) while the other prominent at the later stage of voltages (slope 2). In the low applied voltage range, the maximum slope value is 1.39 (as in the case of pure sample) while the minimum slope value is 1.07 (as in the case of 0.44 wt% CNTs sample). On the other hand, at higher applied voltages the slopes become bigger and vary between 2.94 and 4.08 for samples containing 1.5 and 5 wt% CNTs, respectively. From the obtained slope results and the power law model, one can conclude that the conduction mechanism at low applied voltage range is almost Ohmic while at high applied voltage range it is almost due to trap charge limited. In general, charge conduction consists of the charge injection from the electrode into the polymeric material and the charge transport inside the polymeric material itself. The charge injection mechanism is reasonable when the whole charge conduction is mostly influenced by the charge injection, whereas the charge transport mechanism is suitable when the effect of the injection barrier is negligible compared with the bulk resistance of the material. The former and the latter are called the injection-limited and the bulk-limited conduction, respectively [35].

The dependence of dc conductivity on temperature at different concentrations of CNTs is shown in Fig. 11. The addition of CNTs increases the dc conductivity at room temperature as described before in Fig. 8. Samples loaded with CNTs up to 1.5 Wt% are found to have an activated behavior. This behavior indicates a competition between two mechanisms. One of them acts to increase the electrical conductivity with the temperature by increasing the mobility of charge carriers inside the composite, while the other decreases the conductivity with the temperature due to the thermal expansion of the polymer matrix with respect to the CNTs, which increases the distance between the carbon nanotubes [36].

In case of low CNTs contents, the activated behavior can be divided into two regions: region I (at low temperature range) and region II (at high temperature range), as shown in Fig. 11. This activated behavior is found to obey the well known Arrhenius' relation

$$\sigma_{dc} = \sigma_{odc} \exp\left(\frac{E_a}{kT}\right) \quad (4)$$

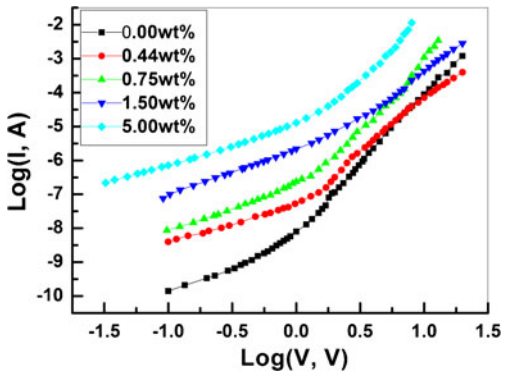

Fig. 10 Plot of log (I) versus log (V) for CNT- P3OT nanocomposites at room temperature

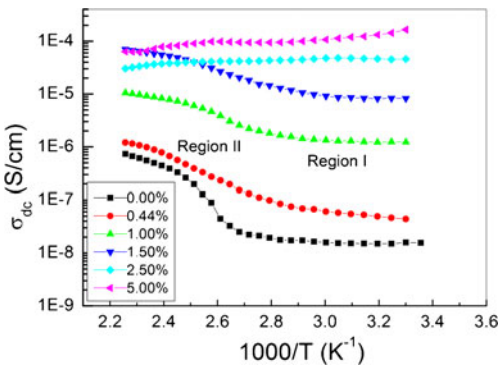

Fig. 11 Temperature dependence of the dc electrical conductivity for CNT- P3OT nanocomposites

Table 1 The calculated values of slope1 (S1), slope2 (S2), and the activation energy (E_a) of CNTs-P3OT nanocomposites

Wt% of CNTs	S1	S2	E_a (eV)
0.00	1.39	4.01	0.93
0.44	1.07	3.20	0.48
0.75	1.26	3.50	0.35
1.50	1.35	2.94	0.31
5.00	1.26	4.08	

where σ_{dc} is the dc conductivity at temperature T, σ_{odc} is the dc conductivity at a certain reference temperature T_o, k is the Boltzmann constant and E_a is the activation energy. The conduction in the first region is mainly due to tunneling through the polymer matrix between conducting sites represented by CNTs as mentioned before. So the activation energy appears to be very small in this region. On the other hand, at higher temperatures (region II) the tunneling mechanism is converted into hopping one. This conversion, however, is attributed to the increase in tunneling paths as a result of thermal expansion and to the increase in the energy of charge carriers with temperature at the same time. A plot between $\ln(\sigma_{dc})$ and 1/T was established independently for all composites at region II (not mentioned here) to determine the values of activation energy in accordance to Eq. 4. The obtained activation energy values were calculated from the known slope values of $\ln(\sigma_{dc})$ versus 1/T and are listed in Table 1. However, these values represent the maximum energy values compared with those determined values at region I. A notable decreasing can be detected in the activation energy (E_a) with increasing CNTs content due to the decrease in the barrier height. Furthermore, increasing of CNTs content over 1.5 wt% will convert the activated behavior into descending one over the whole studied temperature range. At room temperature and at this level of CNTs loadings, CNTs are already attached and the conduction takes place along them. As the temperature increases, thermal expansion of both polymer matrix and CNTs takes place. The great thermal expansion coefficient of polymer over that of CNTs [37] makes the CNTs to be displaced apart and seems to be dispersed rather than attached which appear as a decrease in the electrical conductivity upon heating.

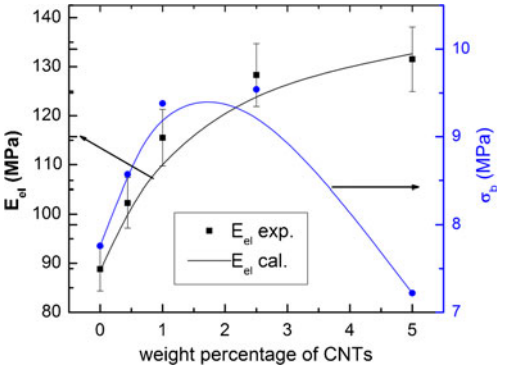

Fig. 13 The elastic modulus and mechanical strength for CNT- P3OT nanocomposites at room temperature

Mechanical properties

The stress strain curves of P3OT loaded with different concentrations of SWCNTs are illustrated in Fig. 12. Initially a viscoelastic response that is considered to be fully reversible is found. For small stresses the material behavior is linear viscoelastic, while with increasing stress the behavior becomes progressively nonlinear. At the yield point the deformation becomes irrecoverable since stress-induced plastic flow sets in leading to a structural evolution which reduces the material's resistance to plastic flow, strain softening.

The origin of the deformation of polymer materials lies in their ability to adjust their chain conformation on a molecular level by rotation around single covalent bonds in the main

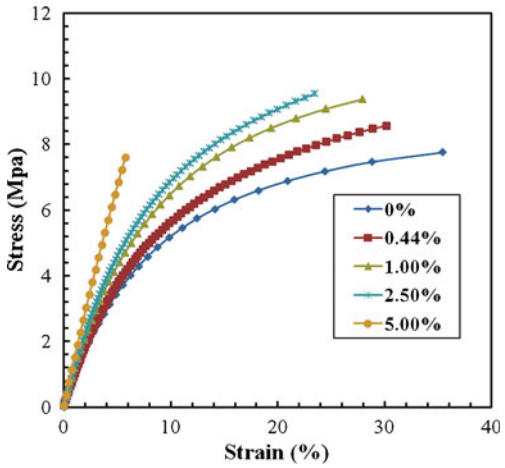

Fig. 12 Stress–strain curves for CNT- P3OT nanocomposites at room temperature and a force rate of 0.5 N/min

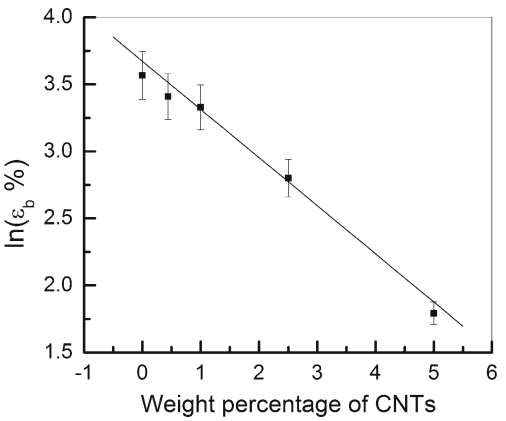

Fig. 14 The natural logarithm of the strain at break for CNT- P3OT nanocomposites at room temperature

chain. This freedom of rotation is, however, controlled by intermolecular (chain stiffness) and intermolecular (interchain) interactions. Together these interactions give rise to an energy barrier that restricts conformational change(s) of the main chain [38]. As the applied stress exceeds this barrier, chain cession takes place resulting as a softening of the material. Before yielding, the straining process is controlled by the rotation of the carbon nanotubes bundles, which act as pseudosprings independent of the strain rate. Yielding occurs when the polymer backbone chains begin to disentangle [39–41].

Separate plots of the change of stress and strain $d\sigma/d\varepsilon$ versus strain ε are performed for all CNTs loadings. It shows strain-independent regions at very low strain values. These constant values are taken to be the elastic modulus (E_{el}) at different CNTs loadings, which are shown in Fig. 13 together with the mechanical strength. Loadings of CNTs up to 2.5 wt% results as an increase in the elastic modulus from 0.89 to 1.31 GPa for unloaded and 5 wt% loaded samples, respectively. This behavior of the elastic modulus may refers to a good homogeneous distribution of CNTs which reveals more interactions between CNTs and polymer chain endings. Besides, at low loadings (less than or equal to 2.5 wt%) with less aggregation makes polymer chains to be folded around the length of less number of nanotubes resulting in a uniform increase in the elastic modulus and the mechanical strength. On the other hand, at high concentrations of CNTs (at 5 wt%) polymer chains are folded around the length of much more nanotubes, due to the aggregation effect, which decreases the interaction between them and results as a decrease in the mechanical strength. The elastic modulus can be described well with an empirical equation of the form

$$E_{el} = E_{elo} + A[1 - B\exp(-\delta C)] \quad (5)$$

where E_{elo}=0.86 Gpa is the elastic modulus for unloaded samples, C is the concentration of carbon nanotubes, A, B and δ are constants equal 0.5, 0.91, and 0.7 Gpa respectively.

The strain at break is also found to be decreased with CNTs content. Also, the natural logarithm of the strain at break is found to be decreased linearly with the increase of CNts loading as shown in Fig. 14 and according to the linear equation

$$ln(\varepsilon_b) = ln\,(\varepsilon_{bo}) - \delta' C \quad (6)$$

where ε_{bo} is elongation at break for unloaded samples=3.6, δ'=0.36 is a constant and C is the weight content of CNTs.

Conclusions

Very interesting results in the optical, electrical and mechanical properties were obtained when the prepared CNTs were added to P3OT polymer matrix. Optical results reveal that the prepared CNTs at 800 °C are mainly SWCNTs. Also, the addition of these nanotubes to P3OT polymer matrix will decrease optical energy gap and enhance the optical absorbance of the polymer matrix. Furthermore, the addition of CNTs to P3OT matrix will enhance the electrical conductivity of P3OT up to four orders of magnitude above the percolation threshold (0.44 wt% CNT) at room temperature. I-V characteristics of nanocomposites reveal that the conduction mechanism depends on the applied voltage, at low applied voltage range the mechanism is almost due to Ohmic while at high applied voltage range it is almost due to trap charge limited. Additionally, at low temperature range and CNTs content, the electrical conduction is controlled by the tunneling mechanism while at high CNTs content, CNTs become percolated. Hopping mechanism appears at high temperature range and the activation energy decreases with CNTs content at this range of temperature due to the increase of charge carrier's energy. Finally, the values of the elastic modulus increase with increasing CNTs content.

Acknowledgements The authors acknowledge the King Abdelaziz City for Science and Technology (KACST), Saudi Arabia for funding and providing the facilities required for this investigation.

References

1. Koizhaiganova RB, Kim HJ, Vasudevan T, Lee MS (2009) Double-walled carbon nanotube (DWCNT)-poly (3-octylthiophene)(P3OT) composites: electrical, optical and structural investigations. Synth Met 159(23–24):2437–2442
2. Qiao Q, Beck J, Lumpkin R, Pretko J, Mcleskey JT (2006) A comparison of fluorine tin oxide and indium tin oxide as the transparent electrode for P3OT/TiO2 solar cells. Sol Energ Mater Sol Cell 90(7–8):1034–1040
3. Palacios Lidón E, Perez García B, Abellán J, Miguel C, Urbina A, Colchero J (2006) Nanoscale characterization of the morphology and electrostatic properties of poly (3 octylthiophene)/graphite nanoparticle blends. Adv Funct Mater 16(15):1975–1984
4. Xu B, Dang S, Han P, Chi M, Liu G, Liu X (2006) Band gaps of two-dimensional photonic crystal structure using conjugated polymer (3-octylthiophenes). Opt Commun 267(2):362–366
5. Zhokhavets U, Goldhahn R, Gobsch G, Schliefke W (2003) Dielectric function and one-dimensional description of the absorption of poly (3-octylthiophene). Synth Met 138(3):491–495
6. Kazukauskas V, Pranaitis M, Cyras V, Sicot L, Kajzar F (2008) Negative mobility dependence on electric field in poly (3-alkylthiophenes) evidenced by the charge extraction by linearly increasing voltage method. Thin Solid Films 516(24):8988–8992
7. Spanggaard H, Krebs FC (2004) A brief history of the development of organic and polymeric photovoltaics. Sol Energ Mater Sol Cell 83(2–3):125–146
8. Solís JC, De la Rosa E, Cabrera EP (2006) Absorption and refractive index changes of poly (3-octylthiophene) under NO 2 gas exposure. Opt Mater 29:167–172
9. Krinichnyi V, Demianets Y, Mironova S (2008) Charge transfer in poly (3-octylthiophene) modified by fullerene derivative. Physica E: Low-dimensional Syst Nanostructure 40(8):2829–2833
10. Monedero MA, Luengo GS, Moreno S, Ortega F, Rubio RG, Prolongo MG, Masegosa RM (1999) Calorimetric and dielectric study of

a blend containing a conductive polymer: poly (3-octylthiophene)+ poly (ethylene-co-vinylacetate). Polymer 40(21):5833–5842
11. Nicho M, Hernández F, Hu H, Medrano G, Guizado M, Guerrero J (2009) Physicochemical and morphological properties of spin-coated poly (3-alkylthiophene) thin films. Sol Energ Mater Sol Cell 93(1):37–40
12. Valentini L, Armentano I, Biagiotti J, Marigo A, Santucci S, Kenny J (2004) AC conductivity of conjugated polymer onto self-assembled aligned carbon nanotubes. Diam Relat Mater 13(2):250–255
13. Lopez-Mata C, Nicho M, Hu H, Cadenas-Pliego G, García-Hernández E (2005) Optical and morphological properties of chemically synthesized poly3-octylthiophene thin films. Thin Solid Films 490(2):189–195
14. Kymakis E, Alexandou I, Amaratunga G (2002) Single-walled carbon nanotube-polymer composites: electrical, optical and structural investigation. Synth Met 127(1–3):59–62
15. Cao Y, Liu Z, Gao X, Yu J, Hu Z (2011) Dynamic rheological properties and microstructures of liquid-crystalline poly (p-phenyleneterephthalamide) solutions in the presence of single-walled carbon nanotubes. J Polym Res 18(2):263–271
16. Kim SD, Kim JW, Im JS, Kim YH, Lee YS (2007) A comparative study on properties of multi-walled carbon nanotubes (MWCNTs) modified with acids and oxyfluorination. J Fluor Chem 128(1):60–64
17. Meng H, Sui G, Fang P, Yang R (2008) Effects of acid-and diamine-modified MWNTs on the mechanical properties and crystallization behavior of polyamide 6. Polymer 49(2):610–620
18. Kymakis E, Amaratunga G (2003) Photovoltaic cells based on dye-sensitisation of single-wall carbon nanotubes in a polymer matrix. Sol Energ Mater Sol Cell 80(4):465–472
19. Spitalsky Z, Tasis D, Papagelis K, Galiotis C (2010) Carbon nanotube-polymer composites: chemistry, processing, mechanical and electrical properties. Prog Polym Sci 35(3):357–401
20. Murakami Y, Miyauchi Y, Chiashi S, Maruyama S (2003) Direct synthesis of high-quality single-walled carbon nanotubes on silicon and quartz substrates. Chem Phys Lett 377(1–2):49–54
21. Unalan HE, Chhowalla M (2005) Investigation of single-walled carbon nanotube growth parameters using alcohol catalytic chemical vapour deposition. Nanotechnology 16:2153
22. Ayesh AS (2010) Electrical and optical characterization of PMMA doped with Y 0.0025 Si 0.025 Ba 0.9725 (Ti (0.9) Sn 0.1) O 3 ceramic. Chin J Polym Sci 28(4):537–546
23. Jeong MS, Byeon CC, Cha OH, Jeong H, Han JH, Choi YC, An KH, Oh KH, Kim KK, Lee YH (2008) Purity measurement of single-walled carbon nanotubes by UV–VIS-NIR absorption spectroscopy and thermogravimetric analysis. Nano 3(2):101
24. Kim DY, Yun YS, Bak H, Cho SY, Jin HJ (2010) Aspect ratio control of acid modified multiwalled carbon nanotubes. Curr Appl Phys 10(4):1046–1052
25. Chen D, Sasaki T, Tang J, Qin LC (2008) Effects of deformation on the electronic structure of a single-walled carbon nanotube bundle. Physical Review B 77(12):125412
26. Ayesh AS, Abdel-Rahem RA (2008) Optical and electrical properties of polycarbonate/MnCl2 composite films. J Plast Film Sheet 24(2):109
27. Burrows P, Bulovic V, Forrest S, Sapochak L, McCarty D, Thompson M (1994) Reliability and degradation of organic light emitting devices. Appl Phys Lett 65(23):2922–2924
28. Antoniadis H, Abkowitz M, Hsieh B (1994) Carrier deep trapping mobility lifetime products in poly (p phenylene vinylene). Appl Phys Lett 65(16):2030–2032
29. Shen Z, Burrows PE, Bulovic V, McCarty DM, Thompson ME, Forrest SR (1996) Temperature dependence of current transport and electroluminescence in vacuum deposited organic light emitting devices. Jpn J Appi Phys 35:L401–L404
30. Blom P, De Jong M, Vleggaar J (1996) Electron and hole transport in poly (p phenylene vinylene) devices. Appl Phys Lett 68 (23):3308–3310
31. Burrows P, Shen Z, Bulovic V, McCarty D, Forrest S, Cronin J, Thompson M (1996) Relationship between electroluminescence and current transport in organic heterojunction light emitting devices. J Appl Phys 79(10):7991–8006
32. Campos R, Kovalev I, Guo Y, Wakili N, Skotheim T (1996) Red electroluminescence from a thin organometallic layer of europium. J Appl Phys 80(12):7144–7150
33. Abkowitz M, Facci J, Rehm J (1998) Direct evaluation of contact injection efficiency into small molecule based transport layers: influence of extrinsic factors. J Appl Phys 83:2670
34. Musa I, Eccleston W, Higgins S (1998) Further analysis of space-charge-limited currents in polybenzo [c] thiophene films. J Appl Phys 83:5558
35. Bunakov A, Lachinov A, Salikhov R (2004) Current voltage characteristics of thin poly (biphenyl 4 ylphthalide) films. Wiley Online Library, p 387–392
36. Abu Abdeen M, Ghani S (2001) Swelling and electrical properties of rubber vulcanizates loaded with paraffin wax. J Appl Polym Sci 81(13):3169–3177
37. Wang S, Liang Z, Gonnet P, Liao YH, Wang B, Zhang C (2007) Effect of nanotube functionalization on the coefficient of thermal expansion of nanocomposites. Adv Funct Mater 17(1):87–92
38. Bauwens Crowet C, Bauwens J, Homes G (1969) Tensile yield stress behavior of glassy polymers. J Polymer Sci Part A 2: Polymer Physics 7(4):735–742
39. Rubatat L, Gebel G, Diat O (2004) Fibrillar structure of Nafion: matching fourier and real space studies of corresponding films and solutions. Macromolecules 37(20):7772–7783
40. Van der Heijden P, Rubatat L, Diat O (2004) Orientation of drawn Nafion at molecular and mesoscopic scales. Macromolecules 37 (14):5327–5336
41. Liu D, Kyriakides S, Case SW, Lesko JJ, Li Y, McGrath JE (2006) Tensile behavior of Nafion and sulfonated poly (arylene ether sulfone) copolymer membranes and its morphological correlations. J Polymer Sci, Part B: Polymer Phys 44(10):1453–1465